Joint MIMO Radar and Communication System Using a PSK-LFM Waveform With TDM and CDM Approaches

Muge Bekar, Chris J. Baker, *Fellow, IEEE*, Edward G. Hoare, *Senior Member, IEEE*, and Marina Gashinova

***Abstract*—In this paper, a new technique which enables communication data to be embedded into multiple-input multiple-output (MIMO) radar waveforms is presented. A linear frequency modulated (LFM) signal is used for radar sensing, and multiple phase-shift keying (PSK) symbols or bit sequences are embedded into the LFM signal for communications. Such waveforms are subsequently used for radar sensing with MIMO beamforming. Orthogonality between transmitters is ensured using either a time-division multiplexing (TDM) or code-division multiplexing (CDM) approach. The performance of these novel techniques is demonstrated through both simulation and experimentation.**

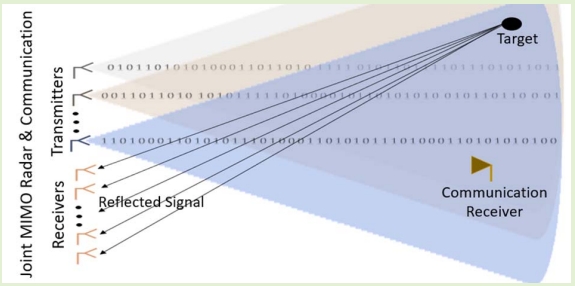

***Index Terms*— Dual function radar and communication, MIMO, PSK-LFM waveform.**

I. Introduction

ADVANCED driver assistance systems (ADAS) have been developed by placing multiple sensors around vehicles in order to aid the human driver when driving and parking. ADAS applications, such as adaptive cruise control, automatic emergency braking, collision warning increase safety of journeys and make it more comfortable. Radar is a compulsory sensor in ADAS because it is the only sensor robust to weather and lighting conditions which directly measures a target's range, angle and radial velocity. Depending on specific ADAS requirements, the detection range of radar is divided into three main groups: long-range radar (LRR) (10-250 m), medium-range radar (MRR) (1-100 m) and short-range radar (SRR) (0.15-30 m) [1]. The commercial standard allocated frequency for LRR is 76-77 GHz whereas it is typically 77-81 GHz for MRR and SRR. Because of the high available bandwidth in the mm-wave frequency bands, automotive radars can have a high range resolution of a few cm.

Manuscript received October 3, 2020; revised November 22, 2020; accepted November 23, 2020. Date of publication December 7, 2020; date of current version February 5, 2021. This work was supported by the Innovate UK (IUK) Project 104268, Cognitive Real Time Sensing System for Autonomous Vehicles (CORTEX). The work of Muge Bekar was supported by the Ministry of National Education, Republic of Turkey. The associate editor coordinating the review of this article and approving it for publication was Prof. Piotr J. Samczynski. *(Corresponding author: Muge Bekar.)*

The authors are with the School of Electronic, Electrical and Systems Engineering, University of Birmingham, Birmingham B15 2TT, U.K. (e-mail: mxo748@student.bham.ac.uk).

Digital Object Identifier 10.1109/JSEN.2020.3043085

Sensors operate over a limited range, a limited field of view and require line of sight, thus limited coverage may compromise vehicle safety [2]. It is, however, possible to enhance situational awareness of the vehicle through the communication of acquired information with other road users, infrastructure etc., within a vehicle-to-everything (V2X) communication network. In today's intelligent transportation system (ITS), a dedicated short-range communication (DSRC) standard of 5.9 GHz is used for vehicular communications. The Federal Communication Commission (FCC) in the US has allocated 75 MHz bandwidth [3] whereas the European Telecommunications Standards Institute (ETSI) has licensed 30 MHz for DSRC [4]. These standards were developed to provide the vehicle-to-vehicle (V2V), vehicle-to-infrastructure (V2I) or vehicle-to-everything (V2X) communications with a maximum data rate of 27 Mbps [5].

Currently, there is strong interest in combining both radar sensing and communications in the same system to use the ElectroMagnetic spectrum more efficiently. Moreover, using one hardware chipset for two different functionalities is a desired approach for vehicles with increasingly dense sensors packaging to provide higher levels of automation. Several methods have been proposed to combine both the radar and communication functions. The first method proposed for automotive applications was the use of spread spectrum techniques [6]. In such an approach, the host vehicle transmits its own pseudo-noise code (PN-code), and the target vehicle re-transmits the signal by multiplying the received signal from the host vehicle with the communication message. Hence, the host vehicle can simultaneously measure the distance

between the host and target vehicle and receive the message by demodulating the received signal from the target vehicle. In [7]–[9], a single transceiver platform which operates in both the radar and communication modes allocating different time slots for each modality was proposed in order to prevent interference between the systems. However, in such an arrangement the radar cannot detect targets during the communication mode, so radar performance may be affected negatively. In the SLIMSENS project [10], [11], a combination of simultaneous 76 GHz long and short-range radar mode and 63 GHz communication mode using a common aperture was considered. In [12]–[15], the authors suggested sending data via modulation of antenna sidelobes, whereas radar detection was via the main lobe. The main drawback of this method is that communication receivers must be always in the sidelobe direction which is not always possible for automotive sensing. Recently a number of research papers were published on dual-function systems where communication waveforms are utilized for joint radar and communication operations. For instance, in [16] IEEE 802.11p standard, allocated for vehicular communication was used in experiments to demonstrate the performance of the targets' range and velocity estimation in two different environments: urban and highway. In [17]–[20] orthogonal frequency-division multiplexing (OFDM) waveforms are used for joint radar and communication purposes. Although use of this waveform does not result in range-Doppler coupling, it requires complex signal processing. In [21]–[23], spread spectrum techniques were employed, but the system design and implementation in terms of time/frequency synchronization is complex and expensive and utilization of spectrum is inefficient. Interest has been shown in using PMCW (Phase Modulated Continuous Wave) for joint radar and communication purposes due to advantages such as a thumbtack-like ambiguity function, robustness to interference and simplicity of implementation [24]–[26]. However, automotive radars require high range resolution as well as high unambiguous range and velocity. In order to satisfy such requirements, the bit duration must be short, and the code length must be large in PMCW.

The majority of automotive radars use chirp signals, and extensive research has been done, where an LFM waveform was used as a signal for encoding communication information. Saddik *et al.* [27] proposed that each transmitted pulse carries one symbol via phased shift keying. In [28] this was extended into the MIMO radar concept by embedding one PSK symbol in each orthogonal waveform. However, this technique achieves very low data rates. In order to increase the data rate, [29]–[31] suggested embedding a sequence of bits into the LFM pulse with the BPSK m-sequence, the minimum shift keying and BPSK respectively. However, in [29] and [31] only communication aspects were considered. In [32], [33], communication sequences were modulated using continuous phase modulation and phase-attached to a polyphase coded frequency-modulated radar waveform. In [34], two different message channels were employed where the binary PSK m-sequence was used to encode a single LFM pulse, and the effect of the code embedding on the radar performance was investigated in terms of the ambiguity function. MIMO beamforming for LFM radar however was not considered in either [29]–[34]. Yet, MIMO beamforming is one of the powerful tools to provide improved angular resolution and improved beam control of modern imaging radar systems designed to deliver situational awareness for semi- and fully-autonomous driving [35].

In this paper, for the first time, we investigate, analytically and experimentally, the feasibility of MIMO PSK modulated LFM waveform dual-function system, where vehicular communication data are embedded into radar waveforms using PSK symbols without significant degradation of radar detection or beamforming performance. To achieve this, the sweep time of the LFM signal is divided into smaller sub-units, and within each sub-units the signal carries a PSK symbol. Hence, multiple symbols are embedded into each chirp. Also, PSK communication can be coded using either an m-sequence or Barker code. In this way, orthogonality of multiple transmitted signals can be maintained so MIMO transmitters can operate simultaneously. The achievable data rate depends on the sub-unit duration, the sweep time, the pulse repetition interval (PRI), the size of the PSK constellation and the number of transmitters operating, which in its turn depends on waveform orthogonality. Importantly, the proposed technique is used in a MIMO configuration in order to gain improved angular resolution. In this paper, orthogonality between MIMO transmitters is provided by TDM and CDM techniques, where each transmitter sends a different message from the others. A message is embedded into an LFM signal using PSK in a TDM implementation and an m-sequence or Barker code is utilized to embed signals into an LFM waveform in a CDM case. These methods are compared, through both simulation and experimentation to assess their radar and communication performance.

To demonstrate the viability of the concept, the experiments were conducted at a frequency of 2 GHz, due to available laboratory equipment. However, without loss of generality the results are scalable to automotive radar frequencies (24 GHz, 77 GHz and 79 GHz) and beyond.

The rest of this paper is organized as follows. Section II describes the proposed technique mathematically. System parameters based on BER are explained in Section III. The simulation results including ambiguity functions are presented in Section IV, and the experimental results are shown in Section V, where results are also discussed. Finally, conclusions are formulated in Section VI.

II. Proposed Techniques

In this section, specific methods to embed communication data into a radar waveform are presented with the aim of obtaining an enhanced data rate consistent with the needs of vehicular communications. The orthogonality between transmitters in MIMO is provided by using TDM or CDM. The proposed joint radar and communication scenario is demonstrated in Fig. 1. We assume that the radar transmitter and receiver antenna elements are co-located, the radar waveform carries communication data and the communication receiver is located in the far-field.

A. Time Division Multiplexing (TDM)

Here, LFM is used as a radar waveform, with sweep time divided into a number of sub-units as shown in Fig. 2 (a).

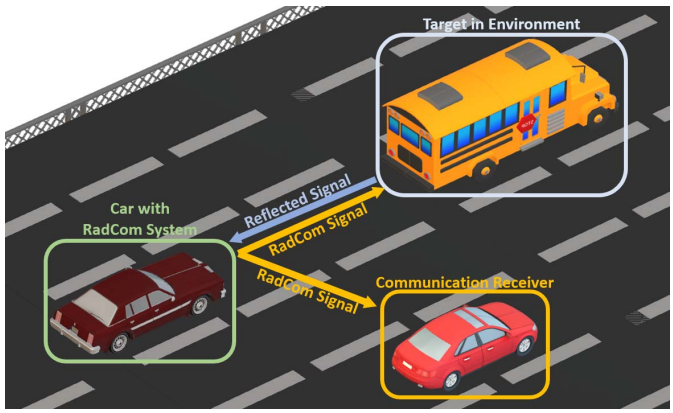

Fig. 1. The proposed joint radar and communication scenario.

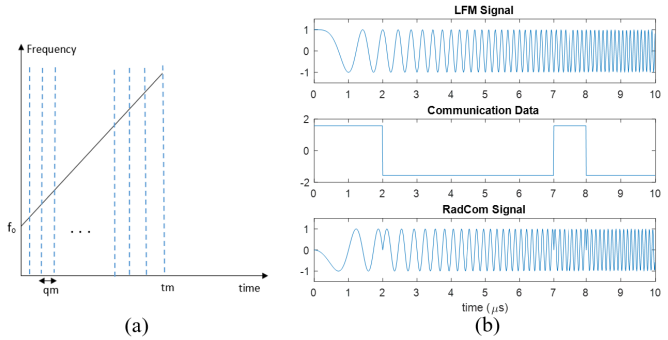

Fig. 2. (a) The demonstration of dividing sweep time into multiple sub-units and (b) an example of embedded data into the radar signal.

The phase of each sub-signal is defined within each sub-unit as illustrated in Fig. 2 (b) according to the chosen phase shift keying modulation such as BPSK, QPSK etc.

The up-chirp LFM signal is given by:

$$s(t) = e^{j(\phi + 2\pi f_c t + \pi \frac{B}{T_m} t^2)}, \quad 0 < t \leq T_m \tag{1}$$

where ϕ is the initial phase, f_c is the center frequency, B is the bandwidth, T_m is the sweep time.

The initial phase, ϕ, is constant during the transmitted signal in a pure LFM signal. However, the phase can be near instantaneously switched at the start of sub-unit segments according to the phase shift modulation sequence of the communication signal. The PSK-LFM signal becomes

$$s_{radcom}(t) = e^{j(\phi_{data}(t) + 2\pi f_c t + \pi \frac{B}{T_m} t^2)}, \quad 0 < t \leq T_m \tag{2}$$

where $\phi_{data}(t)$ is the phase shift keying data which is embedded into LFM signal, and it contains N_{sym} different symbols. N_{sym} is equal to T_m/t_{sub}, and t_{sub} is the sub-unit which expresses the symbol period.

$$\phi_{data}(t) = \begin{cases} \phi[t - i t_{sub}] \in [\,0, 2\pi\,], & i t_{sub} < t \leq (i+1) t_{sub} \\ 0, & \text{otherwise} \end{cases} \tag{3}$$

where $i = 0, 1, \cdots, N_{sym} - 1$, and $\phi_{data}(t)$ depending on PSK constellation will have a finite number of discrete phases, in particularly: two for BPSK and four for QPSK. The dimension of $\phi_{data}(t)$ in discrete time is $(1 \times N_{sample})$, where N_{sample} is the number of samples per pulse.

When a co-located MIMO array is used, orthogonality of transmitted signals must be ensured to avoid mutual interference and here, TDM is utilized. Assuming a MIMO array with N_T transmit and N_R receive antenna elements, the transmit and receive steering vectors, $\boldsymbol{a}(\theta)$ and $\boldsymbol{b}(\theta)$ respectively, are given by

$$\boldsymbol{a}(\theta) = [1 \;\; e^{jkd_T sin\theta} \;\; \cdots \;\; e^{jk(N_T-1)d_T sin\theta}]^T{}_{N_T \times 1} \tag{4}$$

and

$$\boldsymbol{b}(\theta) = [1 \;\; e^{jkd_R sin\theta} \;\; \cdots \;\; e^{jk(N_R-1)d_R sin\theta}]^T{}_{N_R \times 1} \tag{5}$$

where θ is the azimuth angle of the target, k is the wave number $(2\pi/\lambda)$, $[\cdot]^T$ stands for transpose, d_T and d_R are the transmitter and receiver element spacings, respectively.

Each transmitter sends different symbols from the other, and the transmitted data per frame, $\tilde{\boldsymbol{\phi}}_{data_f}(t)$, can be represented as:

$$\tilde{\boldsymbol{\phi}}_{data_f}(t) = [\phi_{data_1}(t) \;\; \phi_{data_2}(t) \;\; \cdots \;\; \phi_{data_{N_T}}(t)]^T \tag{6}$$

where $\phi_{data_n}(t)$ is the transmitted data from n^{th} transmit element, $n = 1, 2, \cdots, N_T$. The dimension of $\tilde{\boldsymbol{\phi}}_{data_f}(t)$ is $(N_T \times N_{sample})$ in discrete time.

Hence, the transmitted signals per frame, $\boldsymbol{s}_{radcom_f}(t)$, can be expressed as

$$\boldsymbol{s}_{radcom_f}(t) = [s_{radcom_1}(t)\; s_{radcom_2}(t) \cdots s_{radcom_{N_T}}(t)]^T \tag{7}$$

where $s_{radcom_n}(t)$ is the transmitted PSK-LFM signal from n^{th} transmit element, $n = 1, 2, \cdots, N_T$. The dimension of $\boldsymbol{s}_{radcom_f}(t)$ is $(N_T \times N_{sample})$ in discrete time.

1) Radar Receiver Part in TDM: In a co-located MIMO radar, at the receiver the signal reflected by L targets is calculated as:

$$\boldsymbol{x}_{rad}(t) = \sum_{l=1}^{L} \beta_l \boldsymbol{b}^c(\theta_l) \boldsymbol{a}^*(\theta_l) e^{j(\tilde{\boldsymbol{\phi}}_{data_f}(t-\tau_l) + 2\pi f_c(t-\tau_l) \ldots + \pi \frac{B}{T_m}(t-\tau_l)^2)} + \epsilon(t) \tag{8}$$

where β_l is the reflection coefficient of the l^{th} target, $\boldsymbol{a}(\theta_l)$ and $\boldsymbol{b}(\theta_l)$ are transmit and receive steering vectors of the l^{th} target, τ_l is the delay time of l^{th} target and $\epsilon(t)$ is zero-mean white Gaussian noise. Symbols $[\cdot]^c$ and $[\cdot]^*$ denote the complex conjugate and the conjugate transpose, respectively. Discrete version of equation (8) will result in $\boldsymbol{x}_{rad}(t)$ being an array of $(N_T N_R \times N_{sample})$.

Each received signal is matched filtered using corresponding transmitted signal as in (9). When a pure LFM signal is used, both matched filtering and stretch processing can be applied to the received signal. Matched filtering only gives the correct range information in the case of PSK-LFM signal.

$$\boldsymbol{y}(t) = \int_0^{T_m} \boldsymbol{x}_{rad}(t) \boldsymbol{s}^c_{radcom_f}(t) d\tau \tag{9}$$

The size of the range compressed data is $(N_T N_R \times N_{sample})$, where $N_T N_R$ is the number of virtual array elements and N_{sample} defines the number of range bins. Finally, a range-angle map is generated by taking a Fourier transform along the azimuth direction.

2) Communication Receiver Part in TDM: It is assumed that communication receiver is in the far-field of the radar transceiver, and contains just one receive element. The received signal at the communication receiver is the time delayed version of the transmitted signal sent from the n^{th} transmit element and is given by

$$\boldsymbol{x}_{com_n}(t) = \boldsymbol{a}_n^*(\theta_c) e^{j(\phi_{data_n}(t-\tau_c)+2\pi f_c(t-\tau_c)+\pi \frac{B}{T_m}(t-\tau_c)^2)} + w(t) \tag{10}$$

where τ_c is the time delay between the transmit antenna and the communication receiver, θ_c is the azimuth angle of the receiver with respect to the transmitter, $w(t)$ is noise.

The received signal is demodulated, using a reference signal as shown in (11). Here, the communication receiver knows the transmitter steering vector, so the reference signal contains the steering vector in order to compensate the phase shifts between the received signals from the MIMO antenna.

$$refsig_{com_n}(t) = e^{j(2\pi f_c t+\pi \frac{B}{T_m}t^2)} \boldsymbol{a}_n^*(\theta_c) \tag{11}$$

In order to demodulate the transmitted data sent from the n^{th} transmit element, a matched filter is used as below.

$$y_n(t) = \int_0^{T_m} x_{com_n}(t) refsig^c_{com_n}(t) d\tau \tag{12}$$

(12) is a matched filter operation presented as a correlation processing. As a result of correlation processing and synchronization the modulation envelope ϕ_{data_n} is extracted.Here, ϕ_{data_n} takes constant values depending on the size of PSK constellation. For instance, if a BPSK modulation is applied, ϕ_{data_n} contains $\pm\pi/2$ values corresponding to each bit. Hence, the resulting term consists of $\pm j$. The transmit data is estimated by using comparator after the integration.

Finally, received data from each transmit element is combined in a vector

$$D = [d_1 \;\; d_2 \;\; \cdots \;\; d_{N_T}] \tag{13}$$

where d_n is the bit from n^{th} transmit element obtained after comparator, and the dimension of D is $(1 \times N_T N_{sym} N_{cons})$. N_{cons} represents the bit number per PSK symbol.

It is an important to note that when a single-input single-output (SISO) antenna configuration is used, the equations above are still valid, but $\boldsymbol{a}(\theta)$ and $\boldsymbol{b}(\theta)$ are equal to one.

B. Code Division Multiplexing (CDM)

Orthogonality of transmit signals can be easily achieved by using TDM, but the data rate is lower than in case of simultaneous transmission. Therefore, we will use CDM approach where quasi-orthogonal signals can be transmitted simultaneously and demodulated in the receiver. Hence, the data rate can be increased by the number of transmitters. Moreover, this provides faster MIMO radar response than TDM.

In CDM, the communication message is embedded into the LFM signal by using different bit sequences for each transmitter. Each sub-unit contains a bit sequence which represents one symbol. To clarify this further, an example is shown in Fig. 3. By using 7-bit m-sequence, the binary symbols are embedded into an LFM signal. The transmitted signals in CDM are given by (14)

$$s_{radcom_n}(t) = e^{j(\phi_{data_n}(t)\Lambda_n(t)+2\pi f_c t+\pi \frac{B}{T_m}t^2)}, \quad 0 < t \le T_m \tag{14}$$

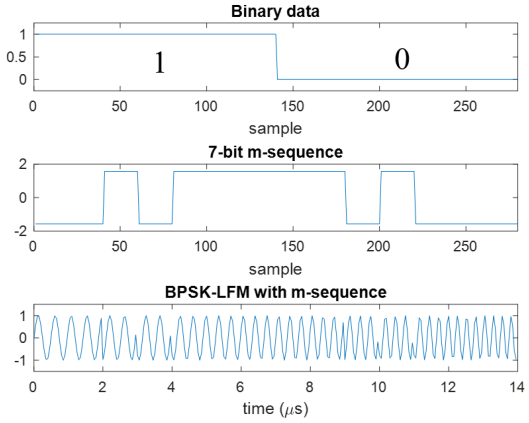

Fig. 3. An example of embedded data into LFM signal by using 7-bit m-sequence.

where $\Lambda_n(t)$ is the bit sequence from n^{th} transmitter with phases of $\pm\pi/2$ and it is repeated each sub-unit time (t_{sub}). $\phi_{data_n}(t)$ is 1 for $'1'$ and -1 for $'0'$ each sub-unit time.

The transmitted data and transmitted signals per frame can be expressed as in (6) and (7) respectively.

1) Radar Receiver Part in CDM: As all transmitters are active at the same time in CDM, the received signals can be written as

$$\boldsymbol{x}_{rad}(t) = \sum_{l=1}^{L} \boldsymbol{b}^c(\theta_l) \sum_{n=1}^{N_T} \beta_l \boldsymbol{a}_n^*(\theta_l) e^{j(\phi_{data_n(t-\tau_l)}\Lambda_n(t-\tau_l)} \ldots^{+2\pi f_c(t-\tau_l)+\pi \frac{B}{T_m}(t-\tau_l)^2)} + \epsilon(t) \tag{15}$$

where all symbols have the same meaning as in (8). The dimension of $\boldsymbol{x}_{rad}(t)$ is $(N_R \times N_{sample})$ in discrete time.

Each received signal is matched filtered using each transmitted signal, so the range response is obtained. Then, range-angle map is created by taking a second Fourier transform in azimuth direction.

2) Communication Receiver Part in CDM: The communication received signal in CDM is summation of the time delayed versions of all transmitted signals, and it is given by

$$x_{com}(t) = \sum_{n=1}^{N_T} \boldsymbol{a}_n^*(\theta_c) e^{j(\phi_{data_n}(t-\tau_c)\Lambda_n(t-\tau_c)} \ldots^{+2\pi f_c(t-\tau_c)+\pi \frac{B}{T_m}(t-\tau_c)^2)} + w(t) \tag{16}$$

where all symbols have the same meaning as in (10).

The received signal is demodulated, using reference signals as shown below. Here the bit sequences used by the transmitters are assumed to be known by the communication receiver.

$$refsig_{com_n}(t) = e^{j(\Lambda_n(t)+2\pi f_c t+\pi \frac{B}{T_m}t^2)} \boldsymbol{a}_n^*(\theta_c) \tag{17}$$

In order to obtain message from received signal, matched filters are utilized as in (12). Moreover, received message from each transmitter is combined as in (13).

III. System Parameters Based on BER

The BPSK-LFM signal is examined in [31] in terms of its bit error rate (BER) performance. It is shown that the BER for BPSK-LFM is exactly the same as that for the

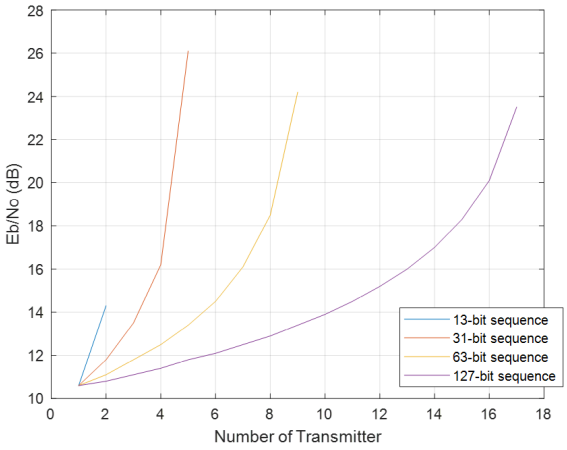

Fig. 4. Number of transmitter vs E_b/N_0 for different code lengths under a 10^{-6} BER or less criterion.

BPSK signal. This means that the carrier waveform does not affect the communication performance in terms of BER. In the TDM case, transmitters emit BPSK-LFM signals in different time slots. Therefore, in the bit error rate (BER) calculation, the TDM system can be thought as a single transmitter. Hence, it can be assumed that multiple transmitter usage with TDM does not change the BER performance of the signal.

With regards to CDM, [36] demonstrates that when one symbol is expressed with a bit sequence, the BER is still the same as for BPSK in the case of single transmitter usage. However, when the number of transmitters increases, the BER response becomes worse. In [36], it is illustrated that there is a trade-off among number of transmitters, code length, energy per bit to noise (E_b/N_0) ratio and BER. The system design can be chosen by trading these parameters. The relationship between these parameters is given in [36] as

$$P_e = Q\left(\frac{1}{\sqrt{\frac{N_T-1}{3N}+\frac{N_0}{2E_b}}}\right) \tag{18}$$

where P_e is the average probability of bit error, $Q(\cdot)$ is Q-function, N_T is the number of transmitter and N is the code length.

In vehicular communication systems, a 10^{-6} BER or less is required. Using this criterion, equation (18) enables E_b/N_0 versus number of transmitters to be plotted as shown in Fig. 4. The graph shows the usable maximum number of transmitters and their required E_b/N_0 for each code lengths. For instance, when a 63-bit code length is used, a maximum of 9 transmitters can be used with minimum E_b/N_0 of 24 dB to obtain the required BER. However, 13 dB E_b/N_0 is enough for 4 transmitters to ensure the BER criterion. Obviously, the longer is the code length, the higher number of transmitters can be used to improve radar performance. In the following sections, we will consider case of only two transmitters, so 13-bit and 31-bit sequences are used in order to prove the CDM concept.

IV. Simulation Results

In this section, the radar and communication performance of both TDM and CDM methods using an example scenario is presented in order to demonstrate the viability of the proposed concept. The radar and communication waveform parameters are shown in Table I. The modulation type used is BPSK, and each pulse contains 500 binary symbols. In this way, data rates of 5 Mbps and 10 Mbps rate are achieved by using TDM and CDM respectively. The data rate can be increased by decreasing the sub-unit duration and/or the PRI, or using a higher size of PSK constellation. Also, increasing the number of transmitters in CDM provides for a higher data rate.

TABLE I
Radar Parameters

Parameters	Value
Frequency	2 GHz
LFM Bandwidth	200 MHz
Sampling Frequency	6.25 Gsps
Sweep Time	50 μs*
PRI	100 μs*
Modulation	BPSK
Sub-unit	0.1 μs*
Number of embedded data per pulse	500
Achieved data rate	5 Mbps (in TDM) 10 Mbps (in CDM)
Number of transmitter	2
Number of receiver	4
Spacing between Rx	$\lambda/2$
Spacing between Tx	$4{\cdot}\lambda/2$
Angular Resolution	$\sim$14.4°
Orthogonality	TDM or CDM

Note: * Here, slightly different sweep time, pulse repetition interval and sub-unit are used in order that the sample number is an integer to design a bit.

In TDM, a BPSK-LFM signal is used as discussed above. For the CDM case, 13-bit Barker code and 31-bit m-sequences with their phase-shifted versions are utilized. In the case of a 13-bit Barker code, the first transmitter uses $[1, 1, 1, 1, 1, -1, -1, 1, 1, -1, 1, -1, 1]$ to embed data onto the LFM signal whereas the second transmitter uses its phase-shifted version, $[1, 1, 1, 1, -1, -1, 1, 1, -1, 1, -1, 1, 1]$. A 31-bit m-sequence is obtained by using a polynomial $f(x) = x^5 + x^3 + 1$. In order to understand the impact of embedding data into an LFM signal, ambiguity functions (AF) of pure LFM, BPSK-LFM, 13-bit Barker and 31-bit m-sequence are computed. As seen from the ambiguity function diagram in Fig. 5, embedding data into LFM signal reduces range-Doppler coupling. As the higher number of sequences are used, AF becomes closer to a thumbtack shape. However, it is use of both 13-bit Barker and 31-bit m-sequences lead to appearance of the grating lobes at around 0.05 μs which corresponds to around 15 m.

Simulation scenario. A point target is placed 7.2 m away from the MIMO antenna at a 10° azimuth angle with respect to boresight. A communication receiver is located at an angle of 30°. Note that both transmitters send different messages from each other. However, the same communication data is used in all simulations to compare the radar responses. Range-angle maps are shown in Figs. 6 – 8 for each of the proposed signals. When all range cuts are examined, it may be seen that there is no difference in the azimuth responses where the 4 dB beamwidth is 14.8°. Although the target's positions are obtained correctly, the range resolutions, defined by different roll-offs from the maximum, are different. The 3 dB range resolutions are approximately 0.72 m, 0.52 m

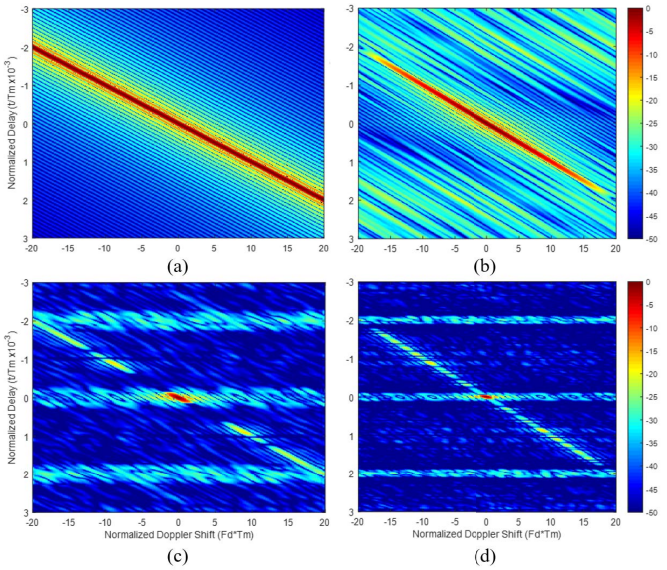

Fig. 5. Ambiguity function of (a) pure-LFM, (b) BPSK-LFM, (c) 13-bit Barker code and its phase-shifted version, (d) 31-bit m-sequence and its phase-shifted version.

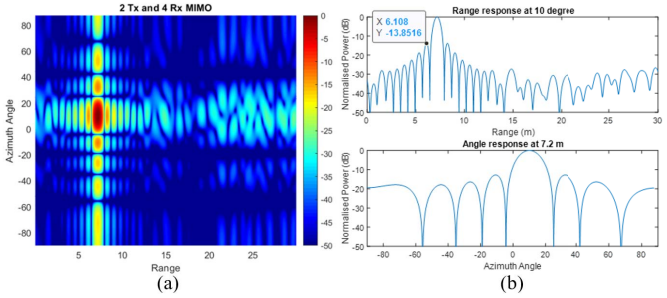

Fig. 6. (a) Range-angle map by using BPSK-LFM, (b) range and azimuth angle cuts.

and 0.32 m for BPSK-LFM, 13-bit Barker code and 31-bit m-sequence cases respectively. The data bandwidth depends on the bit duration. When the null-to-null bandwidths are examined, it can be seen that the data bandwidth can extend the LFM bandwidth. Naturally, the null-to-null bandwidth is close to twice of the total signal bandwidth. For instance, 3.2 ns bit duration is used in 31-bit m-sequence, and this results in a bandwidth of 312.5 MHz. A null-to-null bandwidth of nearly 640 MHz is obtained in the case of 31-bit m-sequence because the data bandwidth is greater than the LFM bandwidth (200 MHz).

On the other hand, the sidelobe level dramatically decreases when using a higher number of bit sequences as seen from the Figs. 6 - 8. BPSK-LFM produces the highest sidelobe levels in range response whereas 31-bit m-sequence and its shifted version experience the lowest sidelobe level, compared with others. Also, when 0.1 μs is used as a sub-time unit, a grating lobe is seen every 15 m. Although the power level of the grating lobe is low, it could result in appearance of false targets. With regards to the communication part, all proposed methods have been examined, and the transmitted message has been received without any distortion (error) in the communication receiver in each case. Therefore, only an

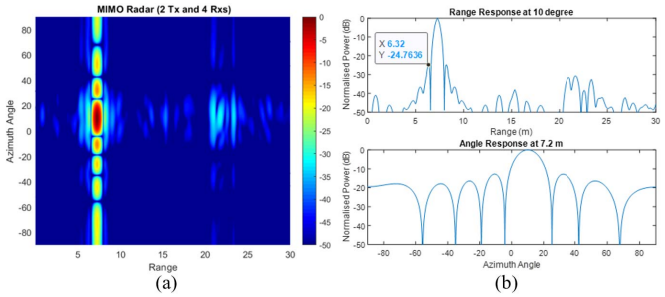

Fig. 7. (a) Range-angle map by using 13-bit Barker code and its shifted version, (b) range and azimuth angle cuts.

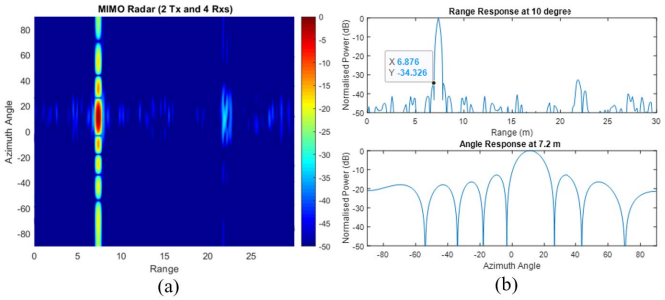

Fig. 8. (a) Range-angle map by using 31-bit m-sequences, (b) range and azimuth angle cuts.

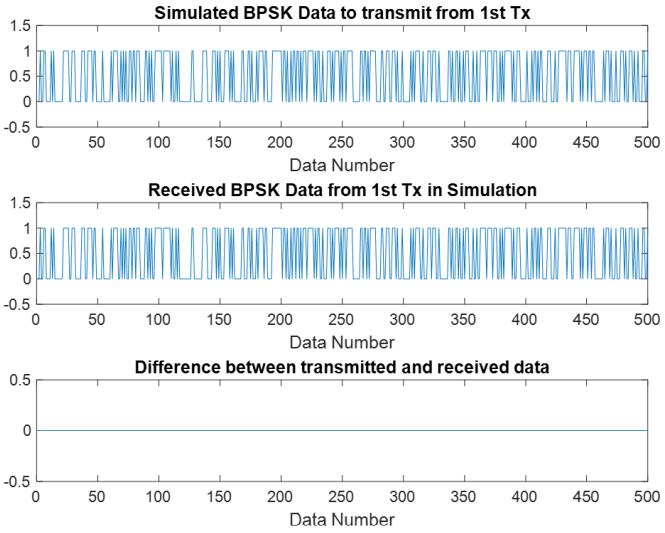

Fig. 9. Simulation result of transmitted data from the first transmitter by using 13-bit Barker code and demodulated data in communication receiver.

example result where signal coded by 13-bit Barker code is transmitted by the first transmitter illustrated in Fig. 9.

V. Experimental Results

To generate and receive modulated signals a Tektronix AWG7102 arbitrary waveform generator and a Tektronix DPO 72004 digital oscilloscope, are used. The oscilloscope sampling rate is limited by 6.25 Gsps, so a 2 GHz carrier was chosen for a signal with a bandwidth of 200 MHz. The parameters of the set-up and signals are given in Table I. Two broadband horn antennas (Q-par WBH1-18S) operating over a range of 1-18 GHz were used, with a physical aperture size of

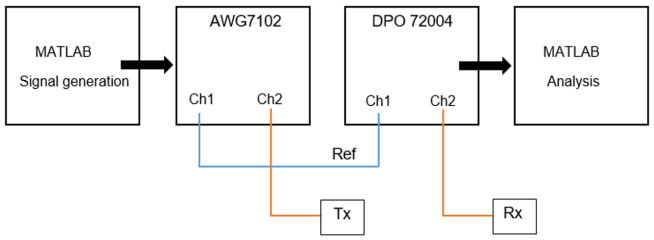

Fig. 10. The configuration of experimental setup.

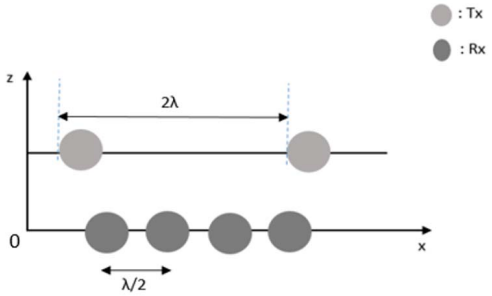

Fig. 11. MIMO array configuration.

96×90 mm^2 [37]. A rectangular corner reflector of $29 \times 29 \times 29$ cm^3 size, made of copper, is used as a calibration target.

The transmitted signals with the parameters given above are simulated in Matlab, then the designed waveform is imported to the AWG. For a full control, a reference signal is provided by cable from the AWG to DPO Channel-1 whereas the target reflected signal is received by DPO Channel-2. The recorded reference and received signals are transferred to a laptop for processing and analysis. The schematic experimental setup is illustrated in Fig. 10. The cable length is 1 m for the reference signal and 4 m cables are used to connect the transmitter and receiver antennas to AWG and DPO respectively.

To emulate 2×4 MIMO array as shown in Fig. 11, the signals were recorded when physical Tx and Rx antennas were positioned at each node of MIMO array sequentially. Orthogonality between received signals is achieved by using TDM and CDM as explained above. Moreover, each transmitted signal contains different messages. The array configuration in Fig. 11 where transmit and receive antennas are off-set in elevation is chosen to accommodate large size antennas are required by MIMO with respect to the signal wavelength.The actual MIMO antenna length of this configuration is $N_R \cdot \frac{\lambda}{2} + 0.09$ m, that is $2\lambda + 0.09 = 0.39$ m where 9 cm relates to the physical antenna size. Hence, the far field distance $d_{far} = \frac{2D^2}{\lambda}$ is 2.028 m. Such MIMO array would yield a beamwidth of approximately 14.4°, according to $\theta_{4dB} = 0.88\frac{\lambda}{D}$ where D is the length of virtual antenna. The target is located at 7 m which includes cable length as illustrated in Fig. 12 (a) at the angle of 10° with respect to the boresight of the antenna array. The communication receiver is placed almost 3.5 m away from the radar antennas at an angle of 30° as shown in Fig. 12 (b). As the experiments with different nodes and CDM and TDM techniques have been conducted in consecutive days, the target position could be slightly different.

During the experiment, one transmit and one receive antenna was used for each measurement simulating one virtual node signal. In order to implement the complete MIMO configuration, for each position of transmit antenna the receive antenna position was shifted by precisely one half-wavelength along the x-axis. After recording the received signal in each receiver position, the transmit antenna position was changed by two wavelengths and the same steps were repeated. This method can be applied when using TDM. For CDM, the received signals at each receiver coming from both transmitters can be summed in the signal processing part. Hence, it can be assumed that transmitters are active simultaneously.

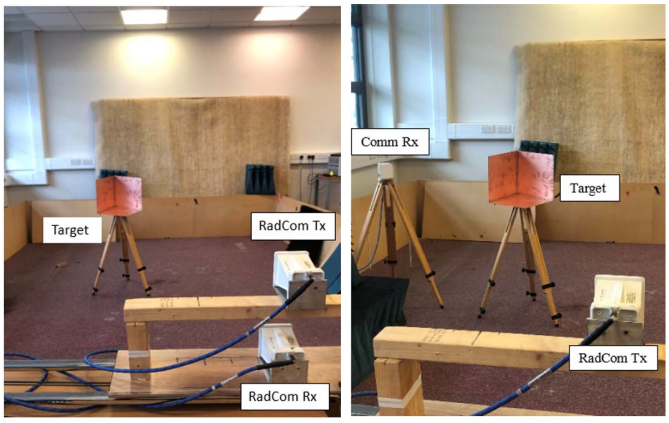

(a) (b)

Fig. 12. (a) Setup for target detection, (b) communication setup.

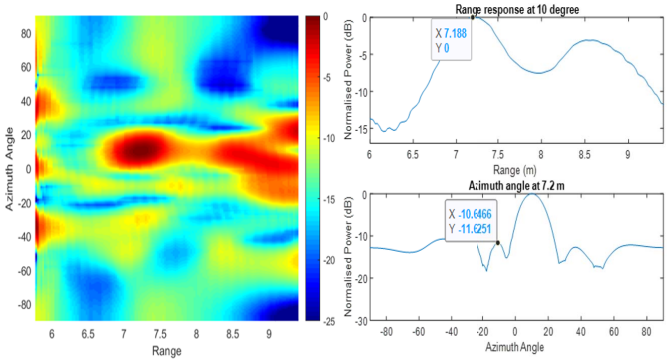

(a) (b)

Fig. 13. Experimental result of BPSK-LFM, (a) Range-azimuth angle map, (b) range and azimuth cuts.

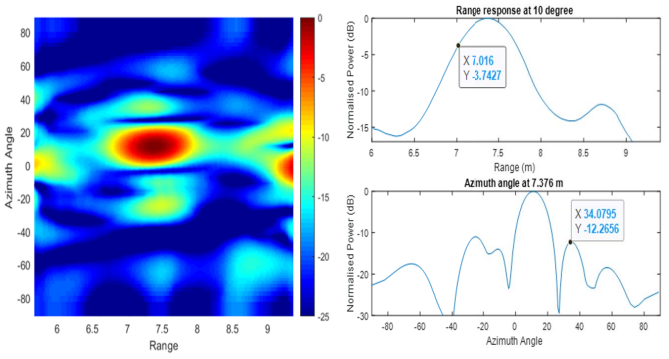

(a) (b)

Fig. 14. Experimental result of 13-bit Barker code, (a) Range-azimuth angle map, (b) range and azimuth cuts.

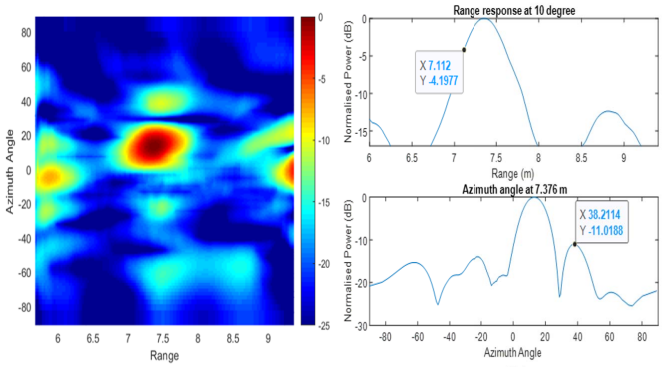

Fig. 15. Experimental result of 31-bit m-sequence, (a) Range-azimuth angle map, (b) range and azimuth cuts.

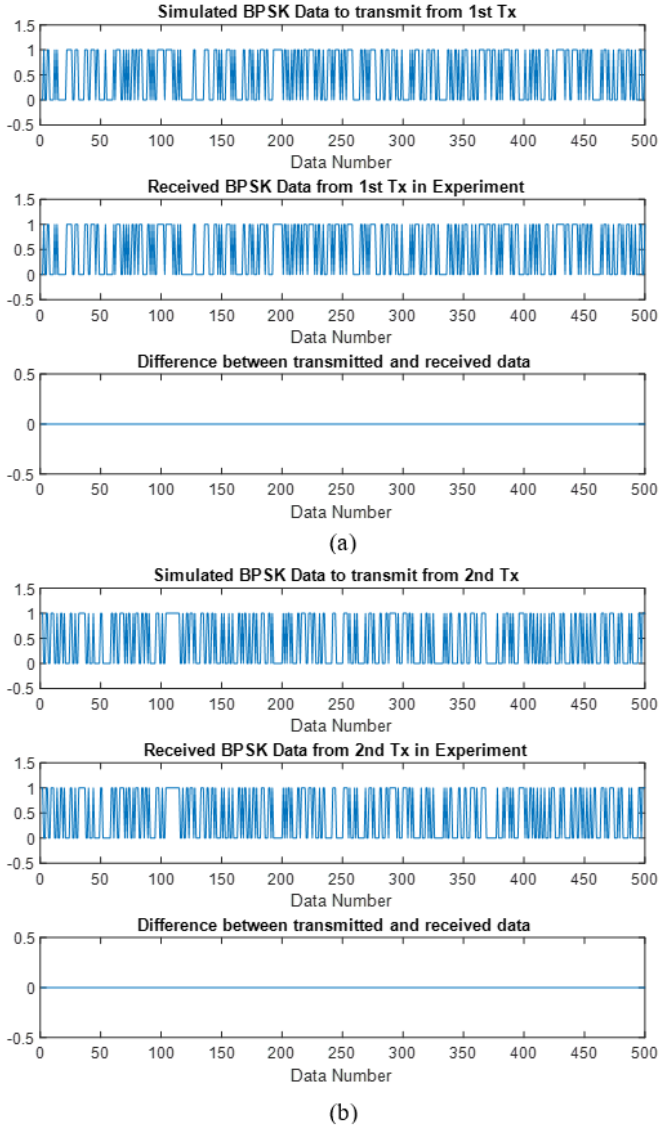

Fig. 16. In experiment (a) transmitted data from the first transmitter by using 13-bit Barker code and demodulated data in communication receiver, (b) transmitted data from the second transmitter by using 13-bit Barker code and the demodulated data in communication receiver.

As only two antennas were available, radar detection and the communication link were done separately. Hence, the radar receiver antenna position was changed to be a communication received antenna after radar detection was completed.

The target appears at 7.2 m in Fig. 13 whereas it appears at around 7.4 m in Fig. 14 – Fig. 15 because it was put in a slightly different position. The range-azimuth angle map is plotted for the range between 5.7 m and 9.4 m. 4-dB azimuth beamwidth is obtained as roughly 15.5° in all experimental results. Range resolutions, however, are different from each other. In the BPSK-LFM, a 0.72 m range resolution is obtained, whereas resolutions of 0.69 m and 0.46 m are obtained from the 13-bit Barker code and 31-bit m-sequence, respectively. Moreover, it is clear that when sequences are used to embed symbols into an LFM signal, the sidelobe levels are less than in case of BPSK-LFM waveform, corresponding to simulation results. Note, the sidelobe patterns are not the same as in the simulation possibly due to multipath/multibounce effects or some inaccuracy in equipment positioning. When the communication part is examined, all data from all transmitters are received by the receiver without any error. Therefore, the example results are shown only for 13-bit Barker code in Fig. 16.

VI. Conclusion

In this paper, we have shown, for the first time, that a dual-mode MIMO waveform can be designed consistent with the parameters anticipated for the future automotive radar systems whilst simultaneously providing high data rate. However, data rate can be varied as a function of the sub-unit duration, sweep time, PRI, the size of the PSK constellation and the number of transmitters operating, which in its turn depends on waveform orthogonality. CDM is better in terms of data rate, though orthogonality is not as good as in TDM and gives rise a slightly higher background level as can be observed in range-Doppler maps. The radar and communication performances of the methods have been investigated by simulation and experiments. It was shown that the range and angular resolution in both simulation and experiments agree well, though the range-angle map results different mostly in terms of sidelobe positions potentially due to multipath effects in small laboratory setting.

References

[1] S. M. Patole, M. Torlak, D. Wang, and M. Ali, "Automotive radars: A review of signal processing techniques," *IEEE Signal Process. Mag.*, vol. 34, no. 2, pp. 22–35, Mar. 2017, doi: 10.1109/MSP.2016.2628914.

[2] J. Choi, V. Va, N. Gonzalez-Prelcic, R. Daniels, C. R. Bhat, and R. W. Heath, "Millimeter-wave vehicular communication to support massive automotive sensing," *IEEE Commun. Mag.*, vol. 54, no. 12, pp. 160–167, Dec. 2016.

[3] J. B. Kenney, "Dedicated short-range communications (DSRC) standards in the united states," *Proc. IEEE*, vol. 99, no. 7, pp. 1162–1182, Jul. 2011.

[4] *2008/671/EC: Commission Decision of 5 August 2008*. Accessed: Dec. 7, 2020. [Online]. Available: https://eur-lex.europa.eu/legal-content/EN/TXT/?uri=CELEX%3A32008D0671

[5] P. Papadimitratos, A. La Fortelle, K. Evenssen, R. Brignolo, and S. Cosenza, "Vehicular communication systems: Enabling technologies, applications, and future outlook on intelligent transportation," *IEEE Commun. Mag.*, vol. 47, no. 11, pp. 84–95, Nov. 2009.

[6] K. Mizui, M. Uchida, and M. Nakagawa, "Vehicle-to-vehicle communication and ranging system using spread spectrum technique (proposal of boomerang transmission system)," in *Proc. IEEE 43rd Veh. Technol. Conf.*, Secaucus, NJ, USA, May 1993, pp. 335–338, doi: 10.1109/VETEC.1993.507206.

[7] K. Konno and S. Koshikawa, "Millimeter-wave dual mode radar for headway control in IVHS," in *IEEE MTT-S Int. Microw. Symp. Dig.*, vol. 3, Denver, CO, USA, Jun. 1997, pp. 1261–1264.

[8] K. Konno and S. Koshikawa, "60 GHz millimeter-wave dual mode radar for IVHS," in *Proc. Top. Symp. Millim. Waves*, Kanagawa, Japan, Jul. 1997, pp. 159–161.

[9] L. Han and K. Wu, "Multifunctional transceiver for future intelligent transportation systems," *IEEE Trans. Microw. Theory Techn.*, vol. 59, no. 7, pp. 1879–1892, Jul. 2011.

[10] R. I. Henderson, W. M. A. Qureshi, and B. Kumar, "A compact multifunction automotive antenna," in *Proc. 2nd Eur. Conf. Antennas Propag. (EuCAP)*, Edinburgh, U.K., Nov. 2007, pp. 1–5, doi: 10.1049/ic.2007.1253.

[11] E. G. Hoare, N. E. Priestley, R. I. Henderson, P. S. Hall, N. J. Clarke, and R. N. Foster, "SLIMSENS, A single aperture 76 GHz automotive radar and 63 GHz communications sensor," in *Proc. JSAE Annu. Congr., Pacifico Conf. Centre*, Yokahama, Japan, May 2008.

[12] J. Euziere, R. Guinvarc'h, M. Lesturgie, B. Uguen, and R. Gillard, "Dual function radar communication time-modulated array," in *Proc. Int. Radar Conf.*, Lille, France, Oct. 2014, pp. 1–4.

[13] P. M. McCormick, S. D. Blunt, and J. G. Metcalf, "Simultaneous radar and communications emissions from a common aperture, part I: Theory," in *Proc. IEEE Radar Conf. (RadarConf)*, Seattle, WA, USA, May 2017, pp. 1685–1690.

[14] P. M. McCormick, B. Ravenscroft, S. D. Blunt, A. J. Duly, and J. G. Metcalf, "Simultaneous radar and communication emissions from a common aperture, part II: Experimentation," in *Proc. IEEE Radar Conf. (RadarConf)*, Seattle, WA, USA, May 2017, pp. 1697–1702.

[15] A. Hassanien, M. G. Amin, Y. D. Zhang, and F. Ahmad, "Dual-function radar-communications: Information embedding using sidelobe control and waveform diversity," *IEEE Trans. Signal Process.*, vol. 64, no. 8, pp. 2168–2181, Apr. 2016.

[16] L. Reichardt, C. Sturm, F. Grunhaupt, and T. Zwick, "Demonstrating the use of the IEEE 802.11P Car-to-Car communication standard for automotive radar," in *Proc. 6th Eur. Conf. Antennas Propag. (EUCAP)*, Mar. 2012, pp. 1576–1580, doi: 10.1109/EuCAP.2012.6206084.

[17] D. Garmatyuk, J. Schuerger, Y. T. Morton, K. Binns, M. Durbin, and J. Kimani, "Feasibility study of a multi-carrier dual-use imaging radar and communication system," in *Proc. Eur. Radar Conf.*, Munich, Germany, Oct. 2007, pp. 194–197.

[18] D. Garmatyuk and J. Schuerger, "Conceptual design of a dual-use radar/communication system based on OFDM," in *Proc. IEEE Mil. Commun. Conf. (MILCOM)*, San Diego, CA, USA, Nov. 2008, pp. 1–7.

[19] C. Sturm, T. Zwick, and W. Wiesbeck, "An OFDM system concept for joint radar and communications operations," in *Proc. IEEE 69th Veh. Technol. Conf. (VTC Spring)*, Barcelona, Spain, Apr. 2009, pp. 1–5.

[20] P. Kumari, D. H. N. Nguyen, and R. W. Heath, "Performance trade-off in an adaptive IEEE 802.11AD waveform design for a joint automotive radar and communication system," in *Proc. IEEE Int. Conf. Acoust., Speech Signal Process. (ICASSP)*, New Orleans, LA, USA, Mar. 2017, pp. 4281–4285.

[21] T. W. Tedesso and R. Romero, "Code shift keying based joint radar and communications for EMCON applications," *Digit. Signal Process.*, vol. 80, pp. 48–56, Sep. 2018.

[22] W. Baxter, E. Aboutanios, and A. Hassanien, "Dual-function MIMO radar-communications via frequency-hopping code selection," in *Proc. 52nd Asilomar Conf. Signals, Syst., Comput.*, Pacific Grove, CA, USA, Oct. 2018, pp. 1126–1130.

[23] I. P. Eedara, A. Hassanien, M. G. Amin, and B. D. Rigling, "Ambiguity function analysis for dual-function radar communications using PSK signaling," in *Proc. 52nd Asilomar Conf. Signals, Syst., Comput.*, Pacific Grove, CA, USA, Oct. 2018, pp. 900–904.

[24] N. Levanon and B. Getz, "Comparison between linear FM and phase-coded CW radars," *IEE Proc.-Radar, Sonar Navigat.*, vol. 141, no. 4, pp. 230–240, Aug. 1994.

[25] S. H. Dokhanchi, M. R. B. Shankar, Y. A. Nijsure, T. Stifter, S. Sedighi, and B. Ottersten, "Joint automotive radar-communications waveform design," in *Proc. IEEE 28th Annu. Int. Symp. Pers., Indoor, Mobile Radio Commun. (PIMRC)*, Montreal, QC, Canada, Oct. 2017, pp. 1–7.

[26] S. H. Dokhanchi, M. R. Bhavani Shankar, K. V. Mishra, T. Stifter, and B. Ottersten, "Performance analysis of mmWave bi-static PMCW-based automotive joint radar-communications system," in *Proc. IEEE Radar Conf. (RadarConf)*, Boston, MA, USA, Apr. 2019, pp. 1–6.

[27] G. N. Saddik, R. S. Singh, and E. R. Brown, "Ultra-wideband multifunctional communications/radar system," *IEEE Trans. Microw. Theory Techn.*, vol. 55, no. 7, pp. 1431–1437, Jul. 2007.

[28] A. Hassanien, M. G. Amin, Y. D. Zhang, and B. Himed, "A dual-function MIMO radar-communications system using PSK modulation," in *Proc. 24th Eur. Signal Process. Conf. (EUSIPCO)*, Budapest, Hungary, Aug. 2016, pp. 1613–1617.

[29] M. Kowatsch and J. Lafferl, "A spread-spectrum concept combining chirp modulation and pseudonoise coding," *IEEE Trans. Commun.*, vol. 31, no. 10, pp. 1133–1142, Oct. 1983.

[30] X. Chen, X. Wang, S. Xu, and J. Zhang, "A novel radar waveform compatible with communication," in *Proc. Int. Conf. Comput. Problem-Solving (ICCP)*, Chengdu, China, Oct. 2011, pp. 177–181.

[31] Z. Zhang, M. J. Nowak, M. Wicks, and Z. Wu, "Bio-inspired RF steganography via linear chirp radar signals," *IEEE Commun. Mag.*, vol. 54, no. 6, pp. 82–86, Jun. 2016, doi: 10.1109/MCOM.2016.7497771.

[32] C. Sahin, J. Jakabosky, P. M. McCormick, J. G. Metcalf, and S. D. Blunt, "A novel approach for embedding communication symbols into physical radar waveforms," in *Proc. IEEE Radar Conf. (RadarConf)*, Seattle, WA, USA, May 2017, pp. 1498–1503.

[33] C. Sahin, J. G. Metcalf, A. Kordik, T. Kendo, and T. Corigliano, "Experimental validation of phase-attached Radar/Communication (PARC) waveforms: Radar performance," in *Proc. Int. Conf. Radar (RADAR)*, Brisbane, QLD, Australia, Aug. 2018, pp. 1–6, doi: 10.1109/RADAR.2018.8557302.

[34] M. Nowak, M. Wicks, Z. Zhang, and Z. Wu, "Co-designed radar-communication using linear frequency modulation waveform," *IEEE Aerosp. Electron. Syst. Mag.*, vol. 31, no. 10, pp. 28–35, Oct. 2016.

[35] A. Stroescu, M. Cherniakov, and M. Gashinova, "Classification of high resolution automotive radar imagery for autonomous driving based on deep neural networks," in *Proc. 20th Int. Radar Symp. (IRS)*, Ulm, Germany, Jun. 2019, pp. 1–10.

[36] T. S. Rappaport, *Wireless Communications: Principles and Practice*. Upper Saddle River, NJ, USA: Prentice-Hall, 2002, ch. 5.

[37] *Miniature Single Polarisation 1–18 GHz Horn Antenna*. Accessed: Dec. 7, 2020. [Online]. Available: http://intermera.ru/files/docs/WBH1-18_Datasheetnew1_web.pdf

Muge Bekar received the B.S. degree in electrical-electronics engineering and mechanical engineering from Erciyes University, Turkey, in 2015 and 2016, respectively, and the M.Sc. degree in RF and microwave engineering from the University of Birmingham, U.K., where she is currently pursuing the Ph.D. degree with the Microwave Integrated Systems Laboratory (MISL). Her research interests include sub-THz automotive radar, wireless communication, and MIMO antenna design.

Chris J. Baker (Fellow, IEEE) holds the University of Birmingham Chair in Intelligent Sensor Systems, and previously, held the position of Chief Technology Officer for Aveillant, a Thales company. Prior to that, he was the Ohio State Research Scholar in Integrated Sensor Systems at the Ohio State University. Until June 2011, he was the Dean and Director of the College of Engineering and Computer Science, Australian National University (ANU). Before that, he held the Thales-Royal Academy of Engineering Chair of Intelligent Radar Systems at University College London. He has been actively engaged in radar systems research since 1984, and is the author of over 300 publications. His research interests include, coherent radar techniques, radar signal processing, radar signal interpretation, electronically scanned radar systems, radar imaging, and natural and cognitive echo locating systems. He was a recipient of the IEE Mountbatten premium (twice) and the IEE Institute premium, and is a Fellow of the IET.

Edward G. Hoare (Senior Member, IEEE) received the Ph.D. degree in over-the-horizon radar from the University of Birmingham. He undertook an apprenticeship at the Royal Radar Establishment, College of Electronics, Malvern, U.K., and after a spell in industry, he joined the School of Electronic, Electrical, and Computer Engineering, University of Birmingham. Since then, he has been involved in teaching, design, and research into radar systems and antennas covering frequencies from 2 MHz to over 670 GHz, including non-co-operative bistatic radar, atmospheric radar acoustic sounding, automotive radar, and low-THz radar. Over the past 12 years, he has provided antenna and millimeter-wave radar consultancy to Jaguar Land Rover and Ford Motor Company. He holds a number of patents in automotive radar. He was a member of the European Automotive Radar Standards Group.

Marina Gashinova received the M.Sc. degree in math from Saint Petersburg State University in 1991, and the Ph.D. degree in physics and math from Saint Petersburg Electrotechnical University, Russia, in 2003. In 2006, she joined the Microwave Integrated System Laboratory (MISL), University of Birmingham (UoB), where she is the Chair of Pervasive Sensing. She is also the Head of the Pervasive Sensing Group, MISL, leading a number of research projects on automotive sensing and THz sensing. Her area of interests include active and passive radar, imaging THz sensing for ground and spaceborne scene assessments, cognitive radar, and deep neural networks classification.